

The non-monotonicity of moist adiabatic warming

Osamu Miyawaki^a

^a *Department of Geosciences, Union College, Schenectady New York, USA*

⁴ *Corresponding author: Osamu Miyawaki, miyawako@union.edu*

1. Introduction

The Clausius-Clapeyron relation implies the potential for a warmer atmosphere to hold more water vapor (Emanuel 1994). This principle is the basis for the positive water vapor feedback (Held and Soden 2000) and various scaling theories in response to warming including extreme precipitation, Hadley cell edge, jet stream position, tropopause height, and CAPE (O’Gorman 2015; Shaw and Voigt 2016; Romps 2016).

In the tropics, convection couples the surface with the free troposphere. Because the timescale of radiative cooling is slower (order of days) compared to convection (order of hours), the tropical atmosphere is to first order in a state of quasi-equilibrium where the climatological free-tropospheric temperature follows a convectively neutral temperature profile set by the surface temperature and humidity Arakawa and Schubert (1974). Although processes like convective entrainment influence the details of this coupling (Miyawaki et al. 2020; Keil et al. 2021), moist adiabatic adjustment serves as a useful first-order approximation (Held 1993). The top-heavy warming profile predicted by moist adiabatic adjustment (Fig. 1b) is a robust feature in climate models and observations, despite historical challenges in observational records (Vallis et al. 2015; Santer et al. 2005).

The top-heavy warming profile predicted by the moist adiabat is important because it increases dry static stability. The spatial variations in the dry static stability response influences the structure of tropical convergence zones because horizontal free-tropospheric gradients, while weak, exist (Neelin and Held 1987; Bao et al. 2022). This structure also defines the tropical lapse rate feedback, a key negative feedback for global climate sensitivity (Hansen et al. 1984). The lapse rate feedback partially cancels the water vapor feedback and scales in tandem because amplified warming in the upper troposphere is a consequence of enhanced latent heat release (Held and Shell 2012). In a moist adiabatic atmosphere that is saturated at the surface, total latent heat release $L_v(q_s^* - q_{\text{top}}^*)$ where L_v is the latent heat of vaporization, q_s^* is surface saturation specific humidity, and q_{top}^* is the cloud top saturation specific humidity. $q_{\text{top}}^* \rightarrow 0$ as $T \rightarrow 0$ in a moist adiabatic atmosphere because the moist adiabat does not predict a stratosphere¹. Thus we expect total latent heat release in a moist adiabatic atmosphere to scale as q_s^* , which increases monotonically with surface temperature as expected from the Clausius-Clapeyron relation (Fig. 1a).

¹Romps (2016) presents a more realistic analysis of how q_{top}^* varies with T_s by assuming a fixed tropopause temperature = 200 K (see Hartmann and Larson 2002; Seeley et al. 2019, for evidence supporting this assumption). q_{top}^* exhibits super Clausius-Clapeyron scaling driven by decreasing cloud top pressure with warming.

Given the monotonic increase in surface specific humidity with surface temperature, one might expect moist adiabatic warming to also increase monotonically with the initial surface temperature at all levels. However, it is a non-monotonic function of initial surface temperature at fixed pressure levels (Fig. 1c, see Appendix A for details on the calculation). This non-monotonicity arises in height coordinates (Fig. A1), with or without latent heat of fusion (see Appendix B and Fig. B1), and across different empirical formula for saturation vapor pressure (see Appendix C and Fig. C1). While previous work has acknowledged the existence of this non-monotonicity (Byrne and O’Gorman 2013; Levine and Boos 2016), an explanation for the non-monotonicity in moist adiabatic warming does not yet exist in the literature.

This raises the question: What physical mechanism drives this non-monotonic warming? Here we derive a thermodynamic explanation for the origin of non-monotonicity in moist adiabatic warming and its cascading effects on buoyancy and vertical velocity.

2. Theory of Non-Monotonic Warming

We start by defining the moist adiabatic temperature profile in pressure coordinates $T(p)$ in terms of the moist adiabatic lapse rate $\Gamma_m = dT/dp$:

$$T(p) = T_s + \int_{p_s}^p \Gamma_m dp' \quad (1)$$

where T_s is surface temperature. We assume the atmosphere is saturated from the surface. The difference between a perturbed and baseline state (Δ) then follows as

$$\Delta T(p) = \Delta T_s + \int_{p_s}^p \Delta \Gamma_m dp' \quad (2)$$

For a small perturbation, $\Delta \Gamma_m$ can be approximated using a first-order Taylor expansion: $\Delta \Gamma_m \approx \frac{d\Gamma_m}{dT_s} \Delta T_s$. Substituting this into Eq. (2) gives:

$$\Delta T(p) \approx \Delta T_s + \left(\int_{p_s}^p \frac{d\Gamma_m}{dT_s} dp' \right) \Delta T_s \quad (3)$$

Thus the non-monotonicity in moist adiabatic warming is encoded into $d\Gamma_m/dT_s$, the sensitivity of the moist adiabatic lapse rate to surface temperature. Indeed, $d\Gamma_m/dT_s$ is non-monotonic




fig-1.png

FIG. 1. (a) Surface saturation specific humidity increases monotonically with surface temperature. (b) Vertical profiles of moist adiabatic warming to a 4 K surface warming, plotted against pressure, for $T_s = 280, 290, 300, 310,$ and 320 K. Warming decreases with initial surface temperature at lower levels while it increases with initial surface temperature at higher levels. (c) Moist adiabatic warming varies non-monotonically with initial surface temperature at all levels, e.g. at 500, 400, 300, and 200 hPa. Moist adiabatic warming peaks at warmer initial surface temperatures at higher levels.

with respect to temperature (dashed line shows the local minima of $d\Gamma_m/dT_s$ in Fig. 2a). Note that $d\Gamma_m/dT_s$ is mostly negative in the troposphere (Fig. 2b). This is consistent with amplified warming aloft because the integral in Eq. (2 is from high to low pressure, which introduces a negative sign.

Γ_m is a function of local state variables $\Gamma_m(T, p)$. Thus to make progress in understanding $d\Gamma_m/dT_s$, we must rewrite $d\Gamma_m/dT_s$ in terms of derivatives with respect to the local state variables (T, p) . To do this we first use the chain rule:

$$\frac{d\Gamma_m}{dT_s} = \left(\frac{\partial \Gamma_m}{\partial T} \right)_p \cdot \frac{dT}{dT_s} + \left(\frac{\partial \Gamma_m}{\partial p} \right)_T \cdot \frac{dp}{dT_s} \quad (4)$$

The second term $\frac{dp}{dT_s} = 0$ because pressure is the vertical coordinate and is an independent variable. Recognizing that by definition $\Gamma_m = \frac{dT}{dp}$,

$$\frac{d}{dp} \left(\frac{dT}{dT_s} \right) = \left(\frac{\partial \Gamma_m}{\partial T} \right)_p \cdot \frac{dT}{dT_s} \quad (5)$$

This is an ordinary differential equation for $\frac{dT}{dT_s}$ as a function of pressure. The solution with the boundary condition $\frac{dT}{dT_s}(p_s) = 1$, is:

$$\frac{dT}{dT_s} = \exp \left(\int_{p_s}^p \left(\frac{\partial \Gamma_m}{\partial T} \right)_p dp' \right) \quad (6)$$

Substituting Eq. (6) back into Eq. (4) gives:

$$\frac{d\Gamma_m}{dT_s} = \left(\frac{\partial \Gamma_m}{\partial T} \right)_p \cdot \exp \left(\int_{p_s}^p \left(\frac{\partial \Gamma_m}{\partial T} \right)_{p'} dp' \right) \quad (7)$$

where $(\partial \Gamma_m / \partial T)_p$ is the moist adiabatic lapse rate sensitivity to local temperature T at pressure level p . The integral describes how a small surface temperature perturbation dT_s influences Γ_m through the sum of all Γ_m changes that occur below p .

The non-monotonicity can arise from either 1) $(\partial \Gamma_m / \partial T)_p$ being non-monotonic and the integral acting to amplify it or 2) $(\partial \Gamma_m / \partial T)_p$ being monotonic but sign changes in $(\partial \Gamma_m / \partial T)_p$ leads to the integral being non-monotonic. Numerical solutions show that $(\partial \Gamma_m / \partial T)_p$ is non-monotonic (dash-dot line shows the local minima of $d\Gamma_m/dT$ in Fig. 2c), which is further amplified by the integral term (Fig. 2d).

Why is $(\partial \Gamma_m / \partial T)_p$ non-monotonic with T ? To understand this we solve for Γ_m from the first law of thermodynamics for adiabatic, non-precipitating, and reversible ascent of a saturated air parcel,

82 which is equivalent to the conservation of saturation moist static energy:

$$c_p dT - \alpha dp + L_v dq^* = 0 \quad (8)$$

83 where c_p is the specific heat capacity of air at constant pressure, α is specific volume, L_v is the
 84 latent heat of vaporization, and q^* is the saturation specific humidity. We assume 1) $c_p \approx c_{pd}$,
 85 neglecting the role of water of all phases on the specific heat capacity and 2) $\alpha \approx \alpha_d = R_d T / p$,
 86 neglecting the virtual effect of water vapor on density.

87 Use the chain rule to expand dq^* :

$$dq^* = \left(\frac{\partial q^*}{\partial T} \right)_p dT + \left(\frac{\partial q^*}{\partial p} \right)_T dp \quad (9)$$

88 Substituting Eq. (9) into Eq. (8) and rearranging gives

$$\left(c_{pd} + L_v \left(\frac{\partial q^*}{\partial T} \right)_p \right) dT = \left(\alpha_d - L_v \left(\frac{\partial q^*}{\partial p} \right)_T \right) dp \quad (10)$$

89 We can derive closed-form expressions for the q^* derivatives using the Clausius-Clapeyron relation
 90 and Dalton's Law. These q^* derivatives describe the role of phase equilibrium shifts in q^* with T
 91 and p on the effective heat capacity and specific volume of the air parcel, respectively:

$$c_L \equiv L_v \left(\frac{\partial q^*}{\partial T} \right)_p \approx \frac{L_v^2 q^*}{R_v T^2} \quad (11)$$

$$\alpha_L \equiv -L_v \left(\frac{\partial q^*}{\partial p} \right)_T \approx \frac{L_v q^*}{p} \quad (12)$$

92 where the approximation arises from assuming saturation vapor pressure $e^* \ll p$.

93 c_L can be thought of as a latent heat capacity, representing the enhanced thermal inertia due to
 94 the fact that latent heating buffers some of the cooling from expansion. Thus c_L acts to increase
 95 the heat capacity of the air parcel such that it has an effective heat capacity $c_{pd} + c_L$.

96 α_L can be thought of as a latent specific volume, representing the enhanced expansion of air with
 97 ascent due to the fact that lower pressure shifts the phase equilibrium of water to favor the vapor

98 phase over liquid. Thus α_L acts to increase the volume of air such that it has an effective specific
 99 volume $\alpha_d + \alpha_L$.

100 Now solving for the moist adiabatic lapse rate $\Gamma_m = dT/dp$:

$$\Gamma_m = \frac{dT}{dp} = \frac{\alpha_d + \alpha_L}{c_{pd} + c_L} \quad (13)$$

$$= \Gamma_d \cdot \frac{1 + \frac{\alpha_L}{\alpha_d}}{1 + \frac{c_L}{c_{pd}}} \quad (14)$$

101 where $\Gamma_d = \alpha_d/c_{pd}$ is the dry adiabatic lapse rate in pressure coordinates and the two non-
 102 dimensional terms represent the fractional increase in effective heat capacity and specific volume
 103 due to phase equilibrium changes:

$$\tilde{c} = \frac{c_L}{c_{pd}} = \frac{L_v^2 q^*}{c_{pd} R_v T^2} \quad (15)$$

$$\tilde{\alpha} = \frac{\alpha_L}{\alpha_d} = \frac{L_v q^*}{R_d T} = \frac{R_v c_{pd} T}{R_d L_v} \tilde{c} = k \tilde{c} \quad (16)$$

104 Substituting Eq. (15) and Eq. (16) into Eq. (14) gives:

$$\Gamma_m = \Gamma_d \cdot \frac{1 + k \tilde{c}}{1 + \tilde{c}} \quad (17)$$

105 For typical values in Earth's atmosphere ($R_v = 461 \text{ J kg}^{-1} \text{ K}^{-1}$, $R_d = 287 \text{ J kg}^{-1} \text{ K}^{-1}$, $c_{pd} = 1005$
 106 $\text{J kg}^{-1} \text{ K}^{-1}$, $L_v = 2.5 \times 10^6 \text{ J kg}^{-1}$, and $T \in [200, 320] \text{ K}$), the factor $k = \frac{R_v c_{pd} T}{R_d L_v} \in [0.13, 0.21]$.
 107 Thus k is a weak function of temperature and is a quasi-constant of order 10^{-1} . In contrast, \tilde{c} scales
 108 exponentially with temperature (through q^*) and varies from $\tilde{c}(200 \text{ K}) \sim 10^{-4}$ to $\tilde{c}(320 \text{ K}) \sim 10^1$.
 109 Thus the temperature sensitivity of Γ_m is controlled by \tilde{c} . Because Γ_m is bounded between Γ_d
 110 (dry limit, $\tilde{c} \rightarrow 0$) and $k\Gamma_d$ (moist limit, $\tilde{c} \rightarrow \infty$), the magnitude of $\partial\Gamma_m/\partial T$ must peak at some
 111 intermediate \tilde{c} else Γ_m would be unbounded.

112 Where does the magnitude of $\partial\Gamma_m/\partial T$ reach its peak value? To solve this we use the quotient
 113 rule on Eq. (13):

$$\frac{\partial\Gamma_m}{\partial T} = \underbrace{\frac{1}{c_{pd} + c_L} \frac{\partial(\alpha_d + \alpha_L)}{\partial T}}_{\text{latent volume sensitivity}} + \underbrace{\left(-\frac{\alpha_d + \alpha_L}{(c_{pd} + c_L)^2} \frac{\partial c_L}{\partial T} \right)}_{\text{latent heat capacity sensitivity}} \quad (18)$$

The latent volume sensitivity varies monotonically with T_s (Fig. 3a, c). The latent heat capacity sensitivity varies non-monotonically with T_s (Fig. 3b, d). Thus we further decompose the latent heat capacity sensitivity to probe its origin:

$$-\frac{\alpha_d + \alpha_L}{(c_{pd} + c_L)^2} \frac{\partial c_L}{\partial T} = -\frac{1}{p} \cdot (1 + \tilde{\alpha}) \cdot \frac{R_d}{c_{pd}} \frac{\partial \log c_L}{\partial \log T} \cdot f_d \cdot f_L \quad (19)$$

where

$$f_d \equiv c_d / (c_{pd} + c_L) \quad (20)$$

$$f_L \equiv c_L / (c_{pd} + c_L) \quad (21)$$

and $f_d + f_L = 1$. f_d and f_L represent the dry and latent fractions of effective heat capacity.

Eq. (19) shows the latent heat capacity sensitivity is a product of four terms that vary monotonically with T . $\tilde{\alpha} = L_v q^* / (\alpha_d p)$ scales exponentially with T through q^* (red line in Fig. 4a). The fractional change in latent heat capacity to a fractional change in temperature $\partial \log c_L / \partial \log T = L_v / (R_v T) - 2$ so it weakly decreases with T (blue line in Fig. 4a). The product of these two terms is weakly non-monotonic in T with a local minimum where $\tilde{\alpha} \approx R_v T / L_v$ (white line in Fig. 4b). At low T , $\tilde{\alpha}$ is small so the product is dominated by the decrease in $\partial \log c_L / \partial \log T$. At high T , $\tilde{\alpha}$ is large so the product is dominated by the exponential increase in $\tilde{\alpha}$. However, the non-monotonicity of these two terms are not the source of the peak in the magnitude of $\partial \Gamma_m / \partial T$, which requires a local maximum, not a minimum.

The dry fraction of effective heat capacity $f_d = c_{pd} / (c_{pd} + c_L)$ logistically decreases with T because c_{pd} is a constant while latent heat capacity c_L increases exponentially with T through q^* (blue line in Fig. 4c). The latent fraction of effective heat capacity $f_L = c_L / (c_{pd} + c_L)$ logistically increases with T (red line in Fig. 4c). The product $f_d \cdot f_L$ is maximized when $f_d = f_L$, or $c_L = c_{pd}$ (black line in Fig. 4d).

What is the physical intuition behind the peak at $c_L = c_{pd}$? Recall that c_L quantifies the enhancement of effective heat capacity due to latent heat of condensation offsetting adiabatic cooling. The q^* derivative in c_L requires two ingredients: 1) cooling from expansion and 2) water vapor. f_d and f_L represent the fractional availability of the two ingredients. At low T , condensation is limited by the availability of water vapor (red line in Fig. 4c). At high T condensation is limited by adiabatic cooling (blue line in Fig. 4c). The peak in latent heat capacity sensitivity corresponds

to where the availability of cooling and water vapor are equally limiting (black line in Fig. 4c). Thus the non-monotonicity in $\partial\Gamma_m/\partial T$ and moist adiabatic warming arises from the competition between the two limiting factors of condensation.

How well does the condition $c_L = c_{pd}$ capture the actual peak in $\partial\Gamma_m/\partial T$? The theory slightly overpredicts the T_s where the magnitude of $\partial\Gamma_m/\partial T$ peaks (compare solid and dash-dot lines in Fig. 5). This error is due to the weak non-monotonicity in the product $(1 + \tilde{\alpha})R_d/c_{pd}\partial\log(c_L)/\partial\log(T)$ which decreases with pressure (Fig. 4b). The error maximizes at the surface where the theory predicts a peak T_s that is 1.6 K warmer than the true peak T_s .

The error in T_s predicted by the theory and the true peak of Γ_m/dT_s grows with height because the integral term in Eq. (7) amplifies the error in $\partial\Gamma_m/\partial T$ at each level below. This error maximizes at 420 hPa where $c_L = c_{pd}$ predicts a peak T_s that is 2.0 K warmer than the true peak T_s (compare solid and dashed lines in Fig. 5). This error is further compounded for T_s corresponding to the peak of moist adiabatic warming ΔT (Eq. 3), leading to a maximum error of 6.6 K at 420 hPa (compare solid and dotted lines in Fig. 5). Thus the condition $c_L = c_{pd}$ is a useful first-order estimate of T_s where moist adiabatic warming peaks. Importantly the theory successfully captures the shift to warmer peak T_s with height, which is due to the fact that temperature decreases with height and thus the transition from the vapor limited to cooling limited regime occurs at a warmer surface temperature with height.

3. Implications of non-monotonicity in moist adiabatic warming on convection

The non-monotonic warming of a moist adiabat has implications for the dynamics of convection. For example, Romps (2016) showed that parcel buoyancy is a non-monotonic function of surface temperature. Specifically the criterion where B peaks is $\beta = 2c_{pd}$ where

$$\beta = c_{pd} + L_v \frac{\partial q^*}{\partial T} = c_{pd} + c_L \quad (22)$$

Thus the criterion that maximizes B is equivalent to where moist adiabatic warming peaks, $c_{pd} = c_L$. Below, we show this is true if the entrainment parameter $a = PE\epsilon/g^2$ is small and derive a more general criterion that maximizes B .

² PE is precipitation efficiency, ϵ is the fractional entrainment rate, and g is gravitational acceleration. See Romps (2016) for the derivation of the entraining plume model.

fig-2.png

FIG. 2. (a) The sensitivity of the moist adiabatic lapse rate to surface temperature, $d\Gamma_m/dT_s$, varies non-monotonically with surface temperature. (b) $d\Gamma_m/dT_s$ has a local minimum across surface temperature at all pressure levels, e.g. across 500, 400, 300, and 200 hPa. A minimum in $d\Gamma_m/dT_s$ corresponds to a maximum in moist adiabatic warming (Fig. 1b) because the integral bounds in Eq. 3 decreases from p_s to p , which introduces a negative sign. The local minimum shifts toward warmer with surface temperature at higher levels. (c) The sensitivity of the moist adiabatic lapse rate to the local temperature at pressure p , $\partial\Gamma_m/\partial T$, also varies non-monotonically with surface temperature. (d) The integral term in Eq. (7) amplifies the non-monotonicity of $\partial\Gamma_m/\partial T$. (a) is the product of (c) and (d).

Buoyancy B is the normalized virtual temperature (or equivalently, density) difference between the rising parcel $T_{v,p}$ and the environment $T_{v,e}$. Here we neglect the virtual effects of water and we

fig-3.png

FIG. 3. The moist adiabatic lapse rate sensitivity to local temperature T , $\partial\Gamma_d/\partial T$ (Fig. 2c), is decomposed into contributions from (a) the latent volume sensitivity and (b) the latent heat capacity sensitivity following Eq. (18). (c) The latent volume sensitivity monotonically increases with local temperature T across all pressure levels, e.g. across 500, 400, 300, and 200 hPa. (d) The latent heat capacity sensitivity has a local minimum that shifts toward warmer surface temperature at higher levels, consistent with the behavior of $d\Gamma_d/dT_s$ (Fig. 2b).

use standard temperature:

$$B \approx \frac{g}{T_e}(T_p - T_e) \quad (23)$$

As before, we express temperature profiles in terms of T_s and the integral of their respective lapse rates. We assume the parcel follows a moist adiabatic lapse rate, Γ_m , while the environment is

fig-4.png

FIG. 4. The latent volume sensitivity is decomposed into a product of four terms (Eq. 19) that varies monotonically with local temperature T , where local means at pressure p . (a) The latent volume ratio $\tilde{\alpha}$ increases exponentially with local temperature (red line) while the fractional change in latent heat capacity c_L to a fractional change in local temperature T decreases linearly with T (blue line). The product of the two is weakly non-monotonic with T where the product has a local minimum (purple line). (b) The local minimum approximately occurs where $\tilde{\alpha} = R_v T / L_v$ (white line). (c) The latent heat capacity fraction f_L increases logistically with local temperature T (red line) while the dry heat capacity fraction f_d decreases logistically with T (blue line). The product of the two is non-monotonic with T where the product has a local maximum (purple line). (d) The local maximum occurs where $c_L = c_{pd}$ (black line).

neutrally buoyant with respect to an entraining lapse rate, Γ_e following the zero-buoyancy plume model introduced by Singh and O’Gorman (2013).

$$T_p = T_s + \int_{p_s}^p \Gamma_m(p') dp' \quad (24)$$

$$T_e = T_s + \int_{p_s}^p \Gamma_e(p') dp' \quad (25)$$

Substituting Eq. (24) and (25) into the definition of buoyancy Eq. (23) yields:

$$B \approx \frac{g}{T_e} \int_{p_s}^p \delta\Gamma dp' \quad (26)$$

where $\delta\Gamma = \Gamma_e - \Gamma_m$. We use the same entraining plume model as in Romps (2016) but express the lapse rate in pressure coordinates:

$$\Gamma_e = \Gamma_d \cdot \frac{(1+a)\alpha_d + \alpha_L}{(1+a)c_{pd} + c_L} \quad (27)$$

Substituting Eq. (13) and (27) into Eq. (26) and simplifying gives:

$$B = \frac{g}{T_e} \int_{p_s}^p \Gamma_d \cdot \frac{a(1-k)\tilde{c}}{(1+a+\tilde{c})(1+\tilde{c})} dp' \quad (28)$$

If we assume that a does not vary with T_s , T_e increases monotonically with T_s at all p . The origin of the non-monotonicity of B must be in the integrand, $\delta\Gamma$. B depends on T primarily through \tilde{c} , which scales exponentially with T through q^* , whereas Γ_d and k are linear functions of T . In the limit of $\tilde{c} \rightarrow 0$ (cold and dry), $\delta\Gamma$ scales as \tilde{c} , which increases with T . In the limit of $\tilde{c} \rightarrow \infty$ (warm and humid), $\delta\Gamma$ scales as \tilde{c}^{-1} , which decreases with increasing T . Thus the integrand maximizes at some intermediate \tilde{c} .

To solve for the condition that maximizes buoyancy we solve for the \tilde{c} derivative of the integrand $\delta\Gamma$ in Eq. (28) and set it to zero:

$$\frac{d}{d\tilde{c}} \left(\Gamma_d \cdot \frac{a(1-k)\tilde{c}}{(1+a+\tilde{c})(1+\tilde{c})} \right) = 0 \quad (29)$$

206 If we assume that a , k , and Γ_d do not vary with T , the solution to Eq. (29) is

$$\tilde{c}_{\text{peak}} = \sqrt{1+a} \quad (30)$$

207 Thus the condition that maximizes buoyancy is $c_L = \sqrt{1+a}c_{pd}$. In the limit of weak entrainment
 208 $a \rightarrow 0$, this reduces to $c_L = c_{pd}$. In the presence of entrainment, buoyancy peaks at a higher c_L and
 209 thus higher T_s all else equal. Entrainment reduces the latent heat released by the cooling parcel
 210 given the same q^* so it shifts the critical point that separates the vapor limited and cooling limited
 211 regimes toward higher q^* .

212 How important is the factor $\sqrt{1+a}$? For an entrainment rate representative of Earth's current
 213 climate $a = 0.2$, the difference in peak T_s that corresponds to $c_L = c_{pd}$ and $c_L = \sqrt{1+a}c_{pd}$ are
 214 < 1.49 K (compare red and solid black line in Fig. 6a). This difference decreases with height and
 215 becomes negligibly small around the tropopause (e.g., 0.33 K at $p = 100$ hPa), which explains
 216 why the criteria $c_L = c_{pd}$ works well for explaining the non-monotonicity of CAPE (Romps 2016).
 217 However, for stronger entrainment rates and for understanding the non-monotonicity of buoyancy
 218 in the lower troposphere the factor $\sqrt{1+a}$ can be important (e.g., 4.38 K for $a = 0.7$ at the surface;
 219 compare red and solid black line in Fig. 6b).

220 How well do these criteria capture the T_s that maximizes buoyancy across the troposphere? We
 221 will first focus on $\delta\Gamma$, i.e. the integrand in Eq. (26). For $a = 0.2$ both criteria capture the T_s
 222 that corresponds to the peak in $\delta\Gamma$ well (< 1.39 K for $c_L = \sqrt{1+a}c_{pd}$, < 2.87 K for $c_L = c_{pd}$,
 223 compare red and solid black line to dashed line in Fig. 6a). The small error arises even for the
 224 $c_L = \sqrt{1+a}c_{pd}$ criterion because $\Gamma_d(1-k)$ is weakly non-monotonic with T (Γ_d increases with T
 225 and $(1-k)$ decreases with T), which we ignored in order to analytically solve Eq. (29). This error
 226 is amplified as we integrate $\delta\Gamma$ to obtain buoyancy Eq. (26) because the errors in the location of
 227 peak $\delta\Gamma$ from each level below accumulates for the location of peak B compare red and solid black
 228 line to dotted line in Fig. 6a).

229 For a higher entrainment parameter $a = 0.7$ the importance of the factor $\sqrt{1+a}$ becomes clear.
 230 The error in T_s that corresponds to the peak in $\delta\Gamma$ is < 3.39 K for the $c_L = \sqrt{1+a}c_{pd}$ criterion
 231 compared to < 5.83 K for the $c_L = c_{pd}$ criterion (compare red and solid black line to dashed line
 232 in Fig. 6b). The error in T_s that corresponds to the peak in buoyancy is surprisingly lower for the
 233 $c_L = c_{pd}$ criterion (< 3.37 K) compared to the $c_L = \sqrt{1+a}c_{pd}$ criterion (< 4.66 K, compare red

and solid black lines to dotted black line in Fig. 6b). This is because $c_L = c_{pd}$ underpredicts T_s for peak B in the lower troposphere, which offsets the growth of the larger error in peak $\delta\Gamma$ (compare solid black and dotted lines in Fig. 6b). The criteria $c_L = c_{pd}$ predicts the T_s of peak buoyancy better than $c_L = c_{pd}\sqrt{1+a}$ in some cases because of a cancelation of errors rather than for the right physical reason. For example the criteria $c_L = c_{pd}$ predicts no shift in T_s that maximizes B to perturbations in a while the criterion $c_L = \sqrt{1+a}c_{pd}$ captures the shift in peak $\delta\Gamma$ and B toward warmer T_s with increasing entrainment (Fig. 6c).

This non-monotonic behavior of buoyancy extends to the strength of the convective updraft. We model the updraft's specific kinetic energy, $\frac{1}{2}w^2$, using Eq. (1) from Del Genio et al. (2007):

$$\frac{d}{dz} \left(\frac{1}{2} w^2 \right) = a' B(z) - (1 + b') \epsilon(z) w^2 \quad (31)$$

where a' and b' are dimensionless constants. We use $a' = 1/6$ and $b' = 2/3$ following Del Genio et al. (2007). $\epsilon(z)$ is the fractional entrainment rate, which is calculated following Eq. (3) in Romps (2016) with entrainment parameter $a = 0.2$ and precipitation efficiency $PE = 0.35$. Since $w(z)$ is determined by the integral of the net force, which includes buoyancy, we expect the non-monotonic dependence on T_s extends to the vertical velocity profile as well.

Numerically integrating Eq. (31) confirms this expectation. The resulting vertical velocity varies non-monotonically with T_s (Fig. 7b). This leads $w(z)$ becoming more top-heavy with warming, i.e. w decreases in the lower troposphere and increases in the upper troposphere (Fig. 7a).

Are these findings relevant to Earth's atmosphere, where convection is not strictly moist adiabatic and vertical velocity is subject to details and constraints not considered here such as cloud microphysics and radiative cooling? Singh and O'Gorman (2015) shows the 99.99th percentile vertical velocity in CM1 exhibits a response to surface temperature variations that is qualitatively consistent with Eq. (31) (compare our Fig. 7a to their Fig. 2). However, in their model the decrease in vertical velocity with warming is confined to the lower troposphere below $p \approx 900$ hPa whereas Eq. (31) predicts a decrease in vertical velocity with warming over a deeper layer of the atmosphere (e.g., below $z \approx 11$ km at 300 K). Thus to better understand the applicability and robustness of our results we analyzed vertical velocity in 9 convective-resolving models simulating radiative convective equilibrium in a 100 km x 100 km domain from the RCEMIP project (Wing et al.

261 2018). We look at the mean vertical velocity profiles for w exceeding the 99.9th percentile at
262 each height level over the last 25 days of each simulation. The 99.9th percentile corresponds to
263 the fastest 1000 samples of w per level per model. We focus on the strongest convective updrafts
264 because the convective core of the strongest updrafts are most conducive to follow parcel profiles
265 that are close to a moist adiabat (Riehl and Malkus 1958).

266 The vertical velocity profiles from the RCEMIP simulations show diverse $w_{>99.9}$ responses to
267 variations in surface temperature (295, 300, and 305 K, see Fig. 8). Some models exhibit a
268 clear top-heavy shift in $w_{>99.9}$ with warming (e.g., CM1, DAM, UCLA-CRM, UKMO, WRF)
269 accompanied by a decrease in $w_{>99.9}$ in the lower troposphere that is qualitatively consistent with
270 the moist adiabatic theory (Fig. 7a). SAM shows a top-heavy shift in $w_{>99.9}$ without a clear
271 decrease in $w_{>99.9}$ in the lower troposphere. In the remaining models the $w_{>99.9}$ response exhibits
272 non-monotonicity with T_s but the peak $w_{>99.9}$ does not necessarily increase. For example DALES
273 and SCALE predict a non-monotonic response in $w_{>99.9}$ with T_s at $z \approx 8$ km but the peak $w_{>99.9}$
274 weakens from $T_s = 300$ to 305 K. MesoNH also predicts a decrease in peak $w_{>99.9}$ from $T_s = 300$
275 K to 305 K but predicts a non-monotonic response in $w_{>99.9}$ with T_s at $z \approx 3$ km, much lower than
276 in DALES and SCALE. The diversity in responses likely arises from differences in model details
277 such as parameterization schemes for cloud microphysics, radiative transfer, and turbulence in
278 addition to emergent behavior such as convective organization that influence convective dynamics
279 beyond the basic thermodynamic processes considered here. Nonetheless, the presence of non-
280 monotonicity and a shift toward increasingly top-heavy updraft velocity profiles in several models
281 suggest that the underlying mechanism controlling non-monotonicity in moist adiabatic warming
282 may be playing a role in shaping the sensitivity of updraft velocity to surface temperature in models
283 that explicitly resolve convective storms.

fig-5.png

FIG. 5. Surface temperature T_s corresponding to the criteria $c_L = c_{pd}$ (solid), the minimum of the moist
adiabatic lapse rate sensitivity to local temperature $\partial\Gamma_m/\partial T$ (dash dot), the minimum of the moist adiabatic
lapse rate sensitivity to surface temperature $d\Gamma_m/dT_s$ (dashed), and the maximum of moist adiabatic warming
 ΔT (dotted). The theory most accurately captures the T_s corresponding to the minimum of $\partial\Gamma_m/\partial T$. The
discrepancy between the theory and the T_s corresponding to the minimum of $d\Gamma_m/dT_s$ and ΔT are larger because
the error at pressure p is the accumulation of errors at levels below p (see Eq. 7 and 3).




fig-7.png

FIG. 7. (a) Vertical profiles of vertical velocity, calculated by numerically integrating Eq. (31) in height using buoyancy B from Eq. (23). Vertical velocity decreases with surface temperature at lower levels while it increases with surface temperature at higher levels. (b) Vertical velocity varies non-monotonically with surface temperature at all levels, e.g. at 5, 10, 15, and 20 km. Vertical velocity peaks at warmer surface temperatures at higher levels consistent with the behavior of buoyancy (Fig. 6a) and moist adiabatic warming (Fig. 5).

4. Summary and Discussion

Moist adiabatic warming varies non-monotonically with respect to surface temperature. The non-monotonicity arises because of a competition between two limiting factors of condensation: availability of water vapor and adiabatic cooling. At low surface temperatures, condensation is limited by the availability of water vapor and thus moist adiabatic warming scales like Clausius-Clapeyron while at high surface temperatures condensation is limited by adiabatic cooling. The surface temperature where moist adiabatic warming peaks approximately follows $c_L = c_{pd}$, where $c_L = L_v \partial q^* / \partial T$. The non-monotonicity of moist adiabatic warming propagates to buoyancy because buoyancy scales as the difference between an entraining lapse rate and the moist adiabatic lapse rate. The surface temperature where buoyancy peaks approximately follows $c_L = c_{pd} \sqrt{1+a}$, where a is the entrainment parameter as defined in Romps (2016). Finally the non-monotonicity of buoyancy propagates to the vertical velocity profile of convective updrafts. Cloud resolving models simulating radiative convective equilibrium exhibit diverse but qualitatively consistent responses in strong convective updrafts to surface temperature changes.

Seeley and Romps (2016) first noted the importance of the $c_L = c_{pd}$ criteria to explain why buoyancy profiles are top heavy. Buoyancy maximizes where the saturation moist static energy difference between the environment and parcel (δh^*) are expressed as a temperature difference (sensible enthalpy difference, $c_{pd} \delta T$) rather than a humidity difference (latent enthalpy difference, $L_v \delta q^*$). Thus the ratio $\tilde{c} = c_L / c_{pd} = L_v \delta q^* / (c_{pd} \delta T)$ quantifies the transition in the layers of the atmosphere where δh^* is expressed largely in terms of $L_v \delta q^*$ (lower troposphere, where $\tilde{c} \gg 1$) and in terms of $c_{pd} \delta T$ (upper troposphere, where $\tilde{c} \ll 1$). Seeley and Romps (2015) showed that buoyancy at a fixed level varies non-monotonically with surface temperature (see their Fig. 2a) and Romps (2016) explained the non-monotonicity of buoyancy to explain the non-monotonicity of CAPE with surface temperature. Following the same reasoning as in Seeley and Romps (2016), Romps (2016) shows that buoyancy and thus CAPE peaks where $c_L = c_{pd}$. Here we find the same criterion $c_L = c_{pd}$ also explains the non-monotonicity in moist adiabatic warming. We also expand on Romps (2016) by showing that a more general criterion for the T_s corresponding to the peak in buoyancy is $c_L = c_{pd} \sqrt{1+a}$, which reduces to Romps (2016)'s criterion in the limit of zero entrainment. The factor $\sqrt{1+a}$ is insignificant in Earth's current climate (e.g. for $a = 0.2$, $\sqrt{1+a} = 1.09$) thus Romps (2016)'s criterion works well for understanding the non-monotonicity




fig-8.png

FIG. 8. Updraft velocity from 9 cloud resolving models (CM1, DALES, DAM, MesoNH, SAM-CRM, SCALE, UCLA-CRM, UKMO-CASIM, and WRF) that participated in RCEMIP (Wing et al. 2018). The simulations are on a $100 \text{ km} \times 100 \text{ km}$ periodic domain for uniform sea surface temperatures set to 295 (blue), 300 (black), and 305 K (red). Updraft velocity at each level is the mean of vertical velocities w that exceed the 99.9th percentile ($w_{>99.9}$).

336 of CAPE. However, the factor $\sqrt{1+a}$ becomes important for generalizing the theory to stronger
337 entrainment rates and for understanding the non-monotonicity of buoyancy in the lower troposphere.

338 The non-monotonicity of moist adiabatic warming may have additional implications for climate,
339 such as the organization of convection and the large-scale circulation response to warming. For
340 example, ? explain the mechanism behind the $2\% \text{ K}^{-1}$ scaling of the mean and extreme upper-level
341 wind response to warming by assuming the atmosphere is moist adiabatic. The non-monotonicity
342 of moist adiabatic warming would drive a non-monotonic change in the meridional and zonal
343 temperature gradients at fixed height or pressure levels. This could serve as a thermodynamically
344 driven hypothesis for the potential of non-monotonicities to emerge in response surface warming
345 of dynamics such as the jet stream wind, extratropical cyclones, and mean overturning circulations.

346 *Acknowledgments.* I thank Andrew Williams, Jiawei Bao, Jonah Bloch-Johnson, Martin Singh,
347 Stephen Po-Chedley, Nadir Jeevanjee, and two anonymous reviewers for helpful discussions and
348 feedback on the manuscript.

349 *Data availability statement.* All scripts used for analysis and plots in this paper are available at
350 <https://github.com/omiyawaki/miyawaki-2025-nonmonotonic-moist-adiabat>. They
351 will also be archived on Zenodo upon publication.

352 APPENDIX A

353 Calculation of Moist Adiabatic Profiles

354 The moist adiabatic profiles are calculated numerically by assuming that saturation moist static
355 energy h is conserved, where:

$$h = c_p T + g z + L_v q^* \quad (\text{A1})$$

356 Here, T is temperature, z is height, q^* is the saturation specific humidity, g is the acceleration
357 due to gravity, c_p is the specific heat of dry air at constant pressure, and L_v is the latent heat of
358 vaporization. All thermodynamic constants are defined in Table A1. Saturation vapor pressure is
359 calculated using Eq. C1 (Bolton 1980).

360 The calculation proceeds in discrete vertical steps of $\Delta p = 50 \text{ Pa}$). For a given surface temperature
361 (T_s) and surface pressure (p_s), h is first calculated at the surface ($z = 0$) and is held constant over
362 height. At each subsequent pressure step p_{i+1} , the height z_{i+1} is calculated using hydrostatic

balance. Then, a numerical root-finding algorithm (`scipy.optimize.root_scalar` with the Brentq method) is used to find the temperature T_{i+1} that satisfies the condition that the h at $(T_{i+1}, p_{i+1}, z_{i+1})$ is equal to the surface h .

To demonstrate that the non-monotonic warming is independent of the vertical coordinate, the results are also presented in height coordinates (Fig. A1). These profiles are obtained by following the same calculation as above except stepping in uniform intervals $\Delta z = 100$ m. The pressure p_{i+1} at height z_{i+1} is calculated using hydrostatic balance.

fig-a1.png

FIG. A1. The moist adiabatic warming response to a 4 K surface warming in pressure coordinates. (a) Vertical profiles of the temperature response (ΔT) as a function of pressure for surface temperatures (T_s) 280, 290, 300, 310, and 320 K. (b) The warming (ΔT) at 5 km, 10 km, 15 km, and 20 km as a function of T_s . The non-monotonic behavior seen in height coordinates (Fig. 1c) is also evident in pressure coordinates.

APPENDIX B

Effect of Latent Heat of Fusion on Moist Adiabatic Warming

We assess how latent heat of fusion influences the non-monotonicity of moist adiabatic warming. We follow the IFS Cycle 40 approximations as summarized by Flannaghan et al. (2014). The

TABLE A1. Thermodynamic constants used in the calculation of moist adiabatic profiles.

Symbol	Description	Value	Units
g	Acceleration due to gravity	9.81	m s^{-2}
c_p	Specific heat of dry air	1005.7	$\text{J kg}^{-1} \text{K}^{-1}$
R_d	Gas constant for dry air	287.05	$\text{J kg}^{-1} \text{K}^{-1}$
R_v	Gas constant for water vapor	461.5	$\text{J kg}^{-1} \text{K}^{-1}$
ϵ	Ratio of gas constants (R_d/R_v)	0.622	dimensionless
p_s	Surface pressure	1000	hPa
L_v	Latent heat of vaporization	2.501×10^6	J kg^{-1}

fraction of liquid water α varies with T as follows:

$$\alpha(T) = \begin{cases} 0, & T \leq T_{\text{ice}}, \\ \left(\frac{T - T_{\text{ice}}}{T_0 - T_{\text{ice}}} \right)^2 & T_{\text{ice}} < T < T_0, \\ 1 & T \geq T_0, \end{cases} \quad (\text{B1})$$

where $T_{\text{ice}} = 253.15 \text{ K}$ and $T_0 = 273.15 \text{ K}$. Thus all condensate is ice below 253.15 K, all condensate is liquid above 273.15 K, and a quadratic transition occurs in between.

The saturation vapor pressure e^* is the weighted average over liquid (e_ℓ^*) and ice (e_i^*):

$$e^* = \alpha e_\ell^* + (1 - \alpha) e_i^* \quad (\text{B2})$$

The saturation vapor pressure over liquid and ice is:

$$e_{\ell,i}^*(T) = a_1 \exp\left(a_3 \frac{T - T_0}{T - a_4}\right) \quad (\text{B3})$$

where over liquid $a_1 = 611.21 \text{ Pa}$, $a_3 = 17.502$, $a_4 = 32.19 \text{ K}$ (Buck 1981) and over ice $a_1 = 611.21 \text{ Pa}$, $a_3 = 22.587$, $a_4 = -0.7 \text{ K}$ (Alduchov and Eskridge 1996).

The effective latent heat of vaporization $L_e^*(T)$ includes both condensation and fusion:

$$L_e^*(T) = L_v + (1 - \alpha) L_f \quad (\text{B4})$$

where $L_f = 0.334 \times 10^6 \text{ J kg}^{-1}$ is the latent heat of fusion.

387 Moist adiabats including fusion are obtained by solving for T that conserves moist static energy
 388 with the effective latent heat L_e :

$$h = c_{pd}T + gz + L_e q^* \quad (\text{B5})$$

389 The vertical profiles of warming ΔT and the warming at fixed pressure levels versus surface
 390 temperature exhibit similar non-monotonic behavior to the case without fusion (compare Fig. 1
 391 and B1). Latent heat of fusion introduces a secondary local maximum in the warming in the mid
 392 troposphere (500 hPa) due to the additional energy release from fusion. When the secondary peak
 393 is to the right of the primary peak the T_s corresponding to peak warming shifts to colder T_s with
 394 fusion (points below the 1:1 line in Fig. B1). As the secondary peak overlaps with the primary
 395 peak the T_s corresponding to peak warming shifts to warmer T_s with fusion (points above the 1:1
 396 line in Fig. B1). This effect is greatest (6.03 K) at 727 hPa. Since fusion represents a secondary
 397 effect and complicates analytical treatment, we neglect it for the rest of the paper.

402 APPENDIX C

403 Effect of Saturation Vapor Pressure Formula on Moist Adiabatic Warming

404 The calculation of moist adiabatic warming profiles depends on the choice of the saturation vapor
 405 pressure formula. To assess the sensitivity of surface temperatures associated with peak moist
 406 adiabatic warming to different formula we test three formula: Bolton (1980), Goff-Gratch (List
 407 1949), and Murphy and Koop (2005).

408 The Bolton (1980) formula is:

$$e^* = 6.112 \exp\left(\frac{17.67(T - 273.15)}{T - 29.65}\right) \quad [\text{hPa}], \quad (\text{C1})$$

409 The Goff-Gratch formula is:

$$\begin{aligned} \log_{10} e^* = & -7.90298 \left(\frac{373.16}{T} - 1 \right) + 5.02808 \log_{10} \left(\frac{373.16}{T} \right) \\ & - 1.3816 \times 10^{-7} \left(10^{11.344(1-T/373.16)} - 1 \right) \\ & + 8.1328 \times 10^{-3} \left(10^{-3.49149(373.16/T-1)} - 1 \right) \\ & + \log_{10}(1013.246) \quad [\text{hPa}] \quad (\text{C2}) \end{aligned}$$

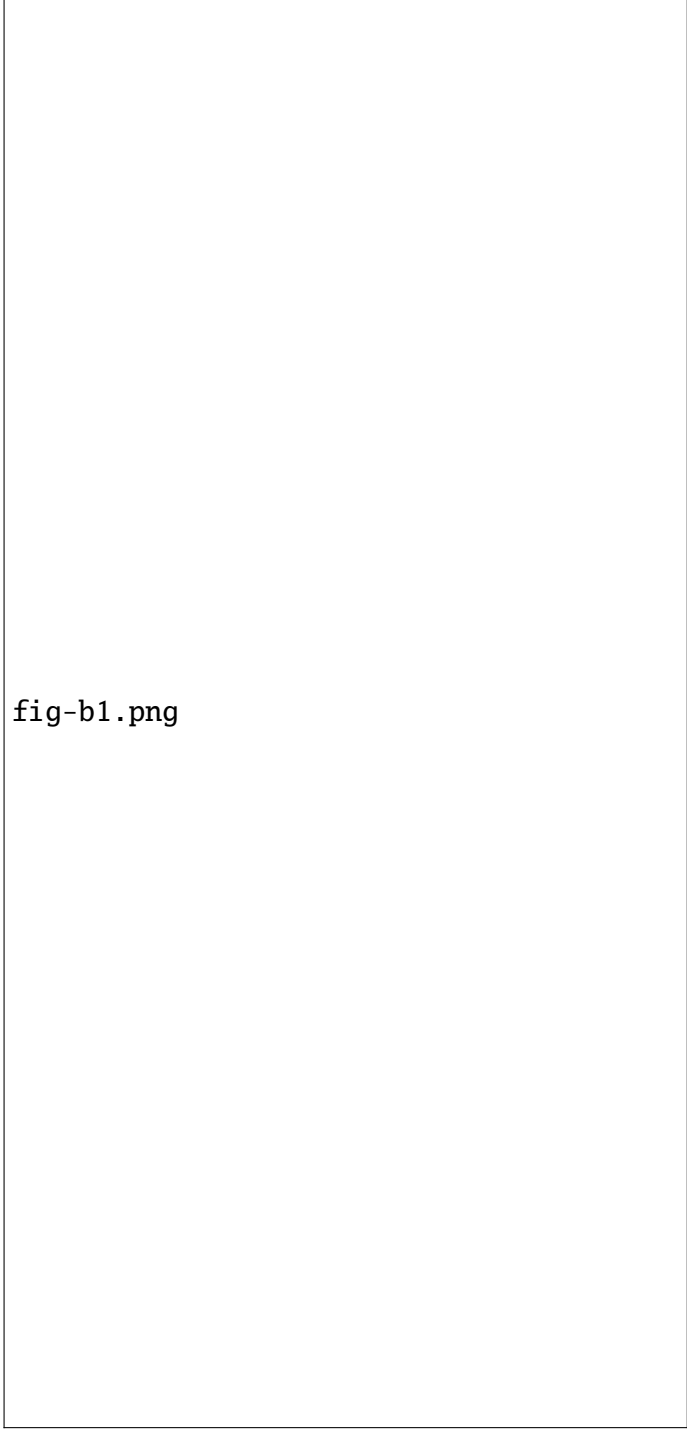


fig-b1.png

398 FIG. B1. The moist adiabatic warming response to a 4 K surface warming with latent heat of fusion. (a)
399 Vertical profiles of the temperature response (ΔT) as a function of pressure for surface temperatures (T_s) of 280,
400 290, 300, 310, and 320 K. (b) The warming (ΔT) at fixed pressure levels of 500, 400, 300, and 200 hPa as a
401 function of T_s . (c) T_s corresponding to peak warming with and without fusion.

The Murphy and Koop (2005) formula is:

$$\ln e^* = 54.842763 - \frac{6763.22}{T} - 4.210 \ln T + 0.000367T + \tanh(0.0415(T - 218.8)) \left(53.878 - \frac{1331.22}{T} - 9.44523 \ln T + 0.014025T \right) \quad [\text{Pa}], \quad (\text{C3})$$

where T is in Kelvin for all 3 formula.

Bolton (1980) is sufficiently accurate for the purposes of evaluating the T_s that leads to maxima in moist adiabatic warming (Fig. C1). The differences in peak T_s across the three saturation vapor pressure formula are small, with the largest deviation being 0.27 K between Bolton and Goff-Gratch and 0.34 K between Bolton and Murphy-Koop. Thus we use Bolton (1980) for the rest of the paper.

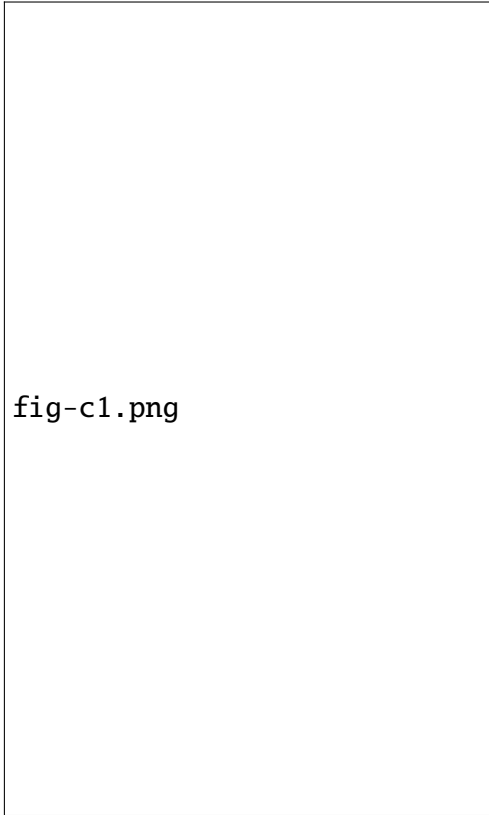


FIG. C1. (a) T_s corresponding to peak warming using Bolton (1980) and Goff-Gratch saturation vapor pressure formula. (b) Same as (a) but comparing Bolton (1980) and Murphy and Koop (2005).

References

- Alduchov, O. A., and R. Eskridge, 1996: Improved magnus form approximation of saturation vapor pressure. *Journal of Applied Meteorology*, **35** (4), 601–609.
- Arakawa, A., and W. H. Schubert, 1974: Interaction of a cumulus cloud ensemble with the large-scale environment, part I. *Journal of the Atmospheric Sciences*, **31** (3), 674–701.
- Bao, J., V. Dixit, and S. C. Sherwood, 2022: Zonal temperature gradients in the tropical free troposphere. *Journal of climate*.
- Bolton, D., 1980: The computation of equivalent potential temperature. *Mon. Weather Rev.*, **108** (7), 1046–1053.
- Buck, A. L., 1981: New equations for computing vapor pressure and enhancement factor. *Journal of Applied Meteorology and Climatology*, **20** (12), 1527–1532.
- Byrne, M. P., and P. A. O’Gorman, 2013: Land–ocean warming contrast over a wide range of climates: Convective quasi-equilibrium theory and idealized simulations. *Journal of climate*, **26** (12), 4000–4016.
- Del Genio, A. D., M.-S. Yao, and J. Jonas, 2007: Will moist convection be stronger in a warmer climate?: CONVECTION STRENGTH IN a WARMER CLIMATE. *Geophys. Res. Lett.*, **34** (16).
- Emanuel, K. A., 1994: *Atmospheric Convection*. Oxford University Press.
- Flannaghan, T. J., S. Fueglistaler, I. M. Held, S. Po-Chedley, B. Wyman, and M. Zhao, 2014: Tropical temperature trends in atmospheric general circulation model simulations and the impact of uncertainties in observed SSTs. *Journal of Geophysical Research, D: Atmospheres*, **119** (23), 13,327–13,337.
- Hansen, J., A. Lacis, D. Rind, G. Russell, P. Stone, I. Fung, R. Ruedy, and J. Lerner, 1984: Climate sensitivity: Analysis of feedback mechanisms. *Climate Processes and Climate Sensitivity*, American Geophysical Union (AGU), 130–163.
- Hartmann, D. L., and K. Larson, 2002: An important constraint on tropical cloud - climate feedback. *Geophysical research letters*, **29** (20), 12–1–12–4.

- 444 Held, I. M., 1993: Large-scale dynamics and global warming. *Bull. Am. Meteorol. Soc.*, **74** (2),
445 228–242.
- 446 Held, I. M., and K. M. Shell, 2012: Using relative humidity as a state variable in climate feedback
447 analysis. *Journal of climate*, **25** (8), 2578–2582.
- 448 Held, I. M., and B. J. Soden, 2000: Water vapor feedback and global warming. *Annual review of*
449 *energy and the environment*, **25** (1), 441–475.
- 450 Keil, P., H. Schmidt, B. Stevens, and J. Bao, 2021: Variations of tropical lapse rates in climate
451 models and their implications for upper tropospheric warming. *Journal of climate*, **34** (24), 1–50.
- 452 Levine, X. J., and W. R. Boos, 2016: A mechanism for the response of the zonally asymmetric
453 subtropical hydrologic cycle to global warming. *J. Clim.*, **29** (21), 7851–7867.
- 454 List, R. J., 1949: Smithsonian meteorological tables. *Smithsonian miscellaneous collections*, **114**,
455 1–521.
- 456 Miyawaki, O., Z. Tan, T. A. Shaw, and M. F. Jansen, 2020: Quantifying key mechanisms that
457 contribute to the deviation of the tropical warming profile from a moist adiabat. *Geophys. Res.*
458 *Lett.*, **47** (20), e2020GL089136.
- 459 Murphy, D. M., and T. Koop, 2005: Review of the vapour pressures of ice and supercooled water
460 for atmospheric applications. *Quarterly journal of the Royal Meteorological Society. Royal*
461 *Meteorological Society (Great Britain)*, **131** (608), 1539–1565.
- 462 Neelin, J. D., and I. M. Held, 1987: Modeling tropical convergence based on the moist static energy
463 budget. *Mon. Weather Rev.*, **115** (1), 3–12.
- 464 O’Gorman, P. A., 2015: Precipitation extremes under climate change. *Current climate change*
465 *reports*, **1** (2), 49–59.
- 466 Riehl, H., and J. S. Malkus, 1958: On the heat balance of the equatorial trough zone. *Geophysica*,
467 **6** (3-4).
- 468 Romps, D. M., 2016: Clausius–Clapeyron scaling of CAPE from analytical solutions to RCE. *J.*
469 *Atmos. Sci.*, **73** (9), 3719–3737.

470 Santer, B. D., and Coauthors, 2005: Amplification of surface temperature trends and variability in
 471 the tropical atmosphere. *Science*, **309 (5740)**, 1551–1556.

472 Seeley, J. T., N. Jeevanjee, and D. M. Romps, 2019: FAT or FiTT: Are anvil clouds or the
 473 tropopause temperature invariant? *Geophysical research letters*, **46 (3)**, 1842–1850.

474 Seeley, J. T., and D. M. Romps, 2015: Why does tropical convective available potential energy
 475 (CAPE) increase with warming? *Geophysical research letters*, **42 (23)**, 10,429–10,437.

476 Seeley, J. T., and D. M. Romps, 2016: Tropical cloud buoyancy is the same in a world with or
 477 without ice. *Geophysical research letters*, **43 (7)**, 3572–3579.

478 Shaw, T. A., and A. Voigt, 2016: What can moist thermodynamics tell us about circulation shifts
 479 in response to uniform warming? *Geophysical research letters*, **43 (9)**, 4566–4575.

480 Singh, M. S., and P. A. O’Gorman, 2013: Influence of entrainment on the thermal stratification
 481 in simulations of radiative-convective equilibrium. *Geophysical research letters*, **40 (16)**, 4398–
 482 4403.

483 Singh, M. S., and P. A. O’Gorman, 2015: Increases in moist-convective updraught velocities with
 484 warming in radiative-convective equilibrium. *Quarterly Journal of the Royal Meteorological*
 485 *Society*, **141 (692)**, 2828–2838.

486 Vallis, G. K., P. Zurita-Gotor, C. Cairns, and J. Kidston, 2015: Response of the large-scale structure
 487 of the atmosphere to global warming. *Quart. J. Roy. Meteor. Soc.*, **141 (690)**, 1479–1501.

488 Wing, A. A., K. A. Reed, M. Satoh, B. Stevens, S. Bony, and T. Ohno, 2018: Radiative–convective
 489 equilibrium model intercomparison project. *Geoscientific Model Development*, **11 (2)**, 793–813.